Jokiniemi, Kimi; Ryynänen, Kaisa; Vähä, Joni; Kankkunen, Elmo; Stadius, Kari; Ryynänen, Jussi

Active Wideband 55-100-GHz Downconversion Mixer in 22-nm FDSOI CMOS

Published in:
2023 IEEE Nordic Circuits and Systems Conference (NorCAS)

DOI:
10.1109/NorCAS58970.2023.10305458

Published: 01/01/2023

Document Version
Peer-reviewed accepted author manuscript, also known as Final accepted manuscript or Post-print

Active Wideband 55-100-GHz Downconversion Mixer in 22-nm FDSOI CMOS

Kimi Jokiniemi, Kaisa Ryynänen, Joni Vähä, Elmo Kankkunen, Kari Stadius, Jussi Ryynänen
Department of Electronics and Nanoengineering, Aalto University, Finland
Email: kimi.jokiniemi@aalto.fi

***Abstract*—This paper presents a wideband active CMOS downconversion mixer for emerging mmWave communication and sensing applications. The designed mixer utilizes transformer coupling between the transconductance stage and switching stage of a classic Gilbert cell mixer to introduce inductive peaking and decouple the stages at DC. This technique efficiently allows the improvement of Gilbert cell mixer bandwidth, gain and linearity. Additionally, the designed mixer structure comprises a transformer-loaded common-source LO buffer and a two-stage wide bandwidth IF amplifier. The complete mixer consumes 33 mW of power from a low 0.8-V supply voltage. The mixer has been implemented with a 22-nm FDSOI CMOS process and its layout area is 0.13 mm^2. The design achieves a measured peak voltage conversion gain of 3.5 dB and particularly a wide 3-dB RF bandwidth from 55 to 100 GHz, covering a range of mmWave bands with a single device. The mixer also demonstrates a wide 10-GHz IF output bandwidth suitable for high channel bandwidth applications, as well as an input 1-dB gain compression point of -6 dBm.**

***Index Terms*—millimeter wave integrated circuits, CMOS, downconversion, active mixer, transformer coupling**

I. Introduction

Due to the rapidly increasing number of wireless communication systems and emerging sensing applications, the demand for wireless millimeter wave (mmWave) radio systems has grown. The mmWave frequency band between 30 GHz and 300 GHz has become increasingly prospective for high data-rate communication applications due to the availability of large, continuous communication bands and reduced interfering applications currently utilizing these frequencies. Frequency band allocations enable large channel bandwidths and a high number of channels for mmWave communication systems, thus enabling high data rates and increased concurrent user capabilities [1]. Advancements in high-frequency CMOS technologies have further rendered mmWave integrated electronics compelling for commercial applications as the well-established technology typically offers better availability, lower manufacturing costs, higher level of integration, and now increasingly competitive performance compared to compound semiconductor technologies conventional in high-frequency applications [2].

This paper presents the design of a 100-GHz wideband active CMOS downconversion mixer in a 22-nm FDSOI CMOS process. A simplified schematic of the mixer is presented in Fig. 1. The designed mixer has a modified Gilbert cell structure with transformer coupling between the mixer stages to introduce inductive peaking and decouple the mixer stages at DC. Typically, the Gilbert cell mixer has relatively high flicker noise and its linearity and gain suffer from low supply voltages typical for nanometer CMOS processes, which motivates the use of highly linear and low-noise passive mixer structures [3]. To overcome these issues, a variety of efficient modifications to the Gilbert cell structure have been presented in published research [4]–[9]. Particularly transformer coupling, which is used in this work, enables competitive wideband mixer operation to cover a wide range of emerging mmWave communication and sensing bands with a single device and good linearity with a low 0.8-V supply voltage.

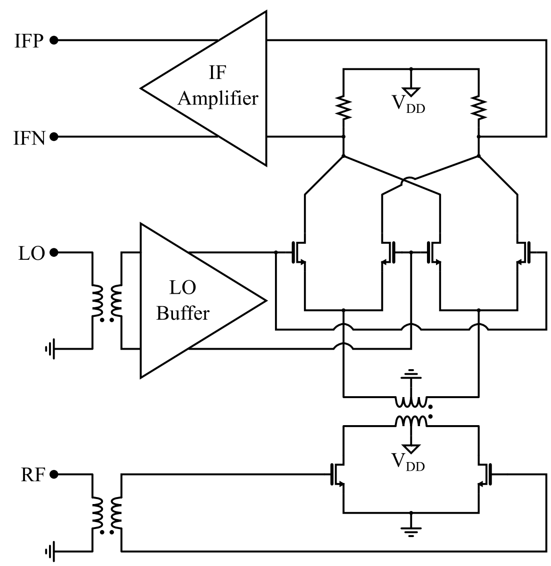

Fig. 1: Simplified schematic of the implemented active mmWave mixer operating at 55-100 GHz frequency range.

This paper presents the design approach for a high-performance active mmWave mixer in detail as follows. Section II presents the use of peaking inductors and optimal biasing of the mixer transistors as two important design techniques to boost the performance of Gilbert-cell-based active mixers and improve their competitiveness at mmWave frequencies. Section III describes the designed mixer beginning with its structure and continuing with its physical implementation. Section IV presents the measurement results of the designed mixer and elaborates on the used measurement arrangements. Finally, Section VI concludes the paper by summarizing the essential achievements of this work.

II. Microwave Mixer Design

This section analyses the use of peaking inductors and discusses appropriate biasing of the active devices. These two methods can significantly improve the performance of an active microwave mixer and thus are worth scrutiny.

A. Peaking Inductors

The Gilbert cell mixer is a classic, widely used double-balanced active mixer topology. A downconverting Gilbert cell consists of a transconductance (Gm) stage performing V-I conversion in the radio frequency (RF) domain, a current switching stage driven by the local oscillator (LO) signal, and a load performing I-V conversion in the intermediate frequency (IF) domain. The conversion gain of a Gilbert cell downconversion mixer follows the equation

$$CG = \left| \frac{V_{out}@f_{IF}}{V_{in}@f_{RF}} \right| = \frac{2}{\pi} g_{m1} R_L, \tag{1}$$

which indicates that conversion gain is a product of the RF input stage transconductance g_{m1}, load resistance R_L, and a factor $2/\pi$ resulting from the frequency conversion in the switching stage. In a downconversion mixer, the most significant pole is formed by the lumped parasitic capacitance at the switching transistor source nodes. When the effect of the parasitic capacitance is taken into account, the mixer transfer function follows the equation

$$H(s) = \frac{V_{out}@f_{IF}}{V_{in}@f_{RF}} = \frac{2}{\pi} g_{m1} R_L \frac{g_{m2}}{g_{m2} + sC_P}, \tag{2}$$

which shows that the parasitic capacitance forms a pole and causes a low-pass response. Switching stage transistor transconductance g_{m2} is the switching stage input conductance as during ideal switching, the transconductance stage sees exactly one conducting transistor drain node at all times.

Peaking inductors are an important design technique at high frequencies. They can be used to compensate parasitic capacitances and to alter circuit bandwidth. Thus, peaking inductors can be utilized in a Gilbert-cell-based downconversion mixer to resonate the critical parasitic capacitance out. Fig. 2 illustrates the lumped parasitic capacitance as well as shunt and series peaking inductance placements in a single-balanced mixer structure for simplicity. Next, the effects of shunt and series peaking inductance configurations are discussed.

A shunt peaking inductor resonates with the parasitic capacitance so that at the resonant frequency, they present a high impedance forcing the transconductance stage output current to flow fully into the switching stage instead of through the parasitic capacitance. With a shunt peaking inductance, mixer transfer function becomes

$$H(s) = \frac{2}{\pi} g_{m1} R_L \frac{s g_{m2}/C_P}{s^2 + s g_{m2}/C_P + 1/(LC_P)}, \tag{3}$$

which indicates a band-pass response peaking at L and C_P shunt resonant frequency tunable by altering the inductor value. Shunt peaking inductors are utilized in mixer designs in [4], [5].

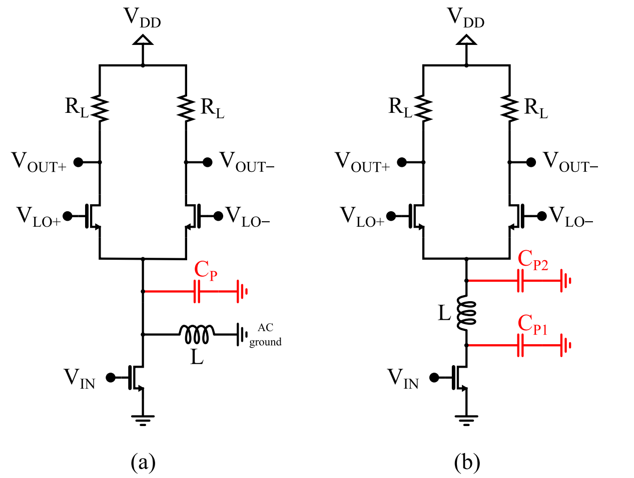

Fig. 2: Single-balanced mixer examples of (a) shunt peaking inductor, (b) series peaking inductor.

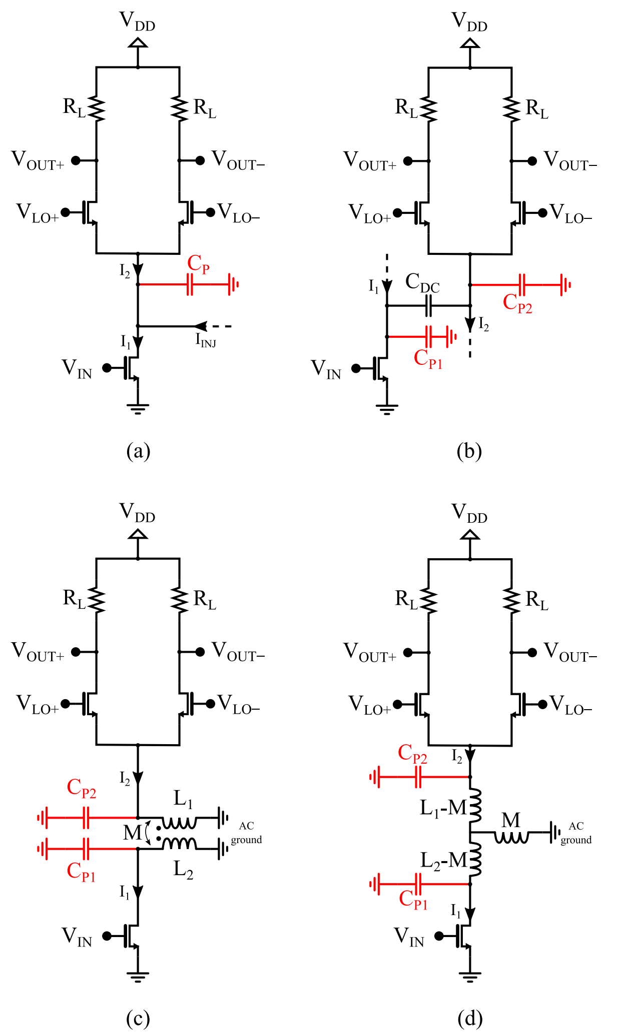

Fig. 3: Single-balanced mixer examples of (a) current injection, (b) capacitive coupling, (c) transformer coupling, and (d) an equivalent AC model of transformer coupling.

A series peaking inductor works by splitting the parasitic capacitance into two and resonating them out [10]. With a series peaking inductance, the mixer transfer function becomes

$$\frac{\frac{2}{\pi}g_{m1}R_Lg_{m2}}{s^3LC_{P1}C_{P2}+s^2LC_{P1}g_{m2}+s(C_{P1}+C_{P2})+g_{m2}}, \quad (4)$$

which is a third-order transfer function and indicates the possibility of two peaks in the frequency response, enabling wider bandwidth. Series peaking inductors are demonstrated in mixers in [6], [11].

B. Individual Mixer Stage Biasing

The Gilbert cell topology has high reverse isolation and LO-RF isolation due to its two cascading transistors. However, the active switching transistors introduce flicker noise and the stacked transistors and a load resistor require considerable voltage headroom, which is often limited in nanometer CMOS processes. Nevertheless, using unequal DC currents at the switching stage and the RF transconductance stage is another important design technique to improve Gilbert cell mixer performance. A higher bias current is desired at the transconductance stage to maximize the transconductance g_{m1} and consequently gain. A lower bias current is desired at the switching stage to lower the voltage drop over the load resistors. Lower switching stage current also decreases the noise contribution of the switching transistors and lowers the overdrive voltage of the switching transistors enabling more abrupt switching [4]. Next, design techniques used to achieve unequal stage biasing are presented.

Fig. 3 presents examples of current injection, capacitive coupling and transformer coupling with single-balanced mixer structures. Injecting current to the transconductance stage with a DC current source structure is one way to achieve unequal bias currents, as used in the mixer designs in [4] and [5] combined with peaking inductors. With current injection, the transistors remain stacked between supply voltages, so headroom improvement with the technique is limited. Additionally, the current source transistors contribute additional parasitic capacitance to the structure. Alternatively, capacitive coupling can be used to decouple mixer stages at DC and bias both stages individually as demonstrated in [4] and [7]. Capacitive coupling allows better voltage headroom improvement in both stages as the mixer structure is folded and transistors are no longer stacked.

Transformer coupling between the transconductance stage and the switching stage is an alternative to capacitive coupling as it also separates the two stages at DC while allowing the AC signal to pass through. Furthermore, a transformer also functions as a shunt-series peaking inductor as shown in the equivalent connection in Fig. 3(d). Therefore transformer coupling enables simultaneous benefits for frequency band tuning, motivating the structure choice in this work. The technique is also demonstrated in designs [8], [9], [12]. The highest bandwidth extension by peaking inductors can be achieved with a combination of shunt and series peaking inductances [10], which however increases circuit complexity and die area. However, a transformer can offer a simpler layout than separate shunt and series peaking inductors due to the overlapping transformer coils.

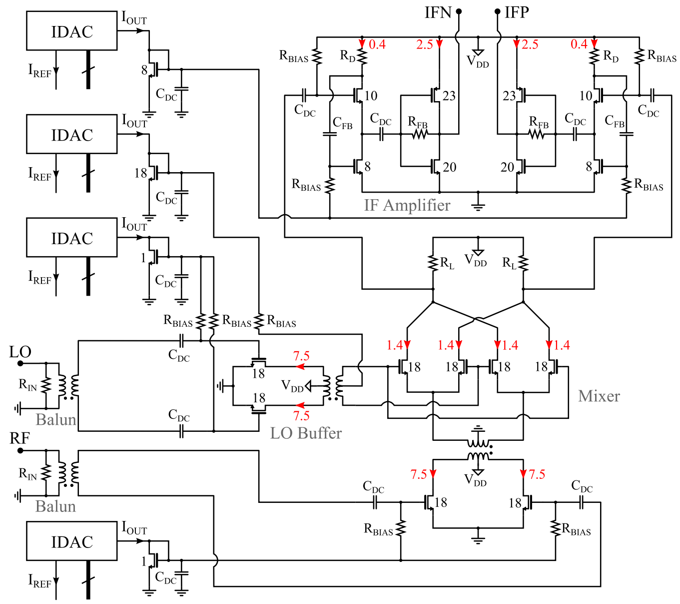

Fig. 4: Full proposed mixer schematic including biasing circuitry. DC current values indicated in mA and transistor widths in μm.

III. Active mmWave Mixer Implementation

The mixer designed in this paper is a modified Gilbert cell mixer with interstage transformer coupling and unequal DC bias currents in the switching and transconductance stages. Fig. 4 shows the complete mixer schematic including biasing circuitry, DC currents, and transistor widths. To minimize gate resistance, transistors in the design use the minimum channel length (20 nm) and a high number of gate fingers. The mixer design uses a super-low threshold voltage variety of transistors to decrease voltage headroom requirements and increase linearity. The technology provides f_T/f_{MAX} values up to 375/290 GHz for NMOS devices making them highly capable for mmWave applications [13]. During this work, circuit simulations have been complemented with electromagnetic field simulations to model the layout parasitic elements with maximal accuracy, and to verify the accuracy of component schematic models at mmWave frequencies.

Transformer coupling used in the proposed mixer is beneficial for increasing gain, bandwidth and linearity and lowering noise as explained in Section II. The interstage transformer center taps are used to bias the switching transistor source nodes to ground and the transconductance transistor drain nodes to V_{DD} = 0.8 V for maximal voltage headroom. The mixer has a fully differential design but the LO and RF input terminals are preceded by single-ended to differential balun transformers to enable single-ended probe measurements. Additionally, 50-Ω shunt matching resistors have been added to the RF and LO inputs to provide input matching with simulated S_{11}<-5 dB on both inputs in the complete mixer frequency band. The transformer-loaded common-source LO buffer provides >3 dB of gain in the frequency band of the mixer with sacrificed gain flatness as a tradeoff. The IF amplifier provides roughly 2 dB of gain, presents a high-impedance load for the mixer, and provides output matching for the 100-Ω differential IF output. The IF amplifier also heavily attenuates spurious output frequency components and LO-IF and RF-IF leakage. The IF amplifier dictates the output frequency band and due to the capacitive coupling between amplifier stages, the IF band does not begin at DC. Thus, the mixer uses a low-IF architecture, which mitigates the effects of baseband flicker noise.

Biasing of the mixer has been done with current mirror configurations instead of classic tail current sources as current mirror connections do not introduce additional transistors stacked between supply voltages and limit mixer transistor voltage headroom. To provide digitally configurable biasing, 5-bit current-mode digital-to-analog converters (IDACs) are used to generate adjustable bias currents for the current mirrors. There are 20 bits in total configuring Gm stage, switching stage, LO buffer, and IF amplifier biasing. Control bits for all the IDACs are transferred onto the chip via on-chip serial peripheral interface (SPI) slave, which performs serial to parallel data conversion and allows an arbitrary number of on-chip configure bits with four signal I/O pads. An off-chip reference current is fed to an additional on-chip NMOS current mirror connection that copies the single reference current for the four IDACs in the mixer.

The mixer layout is presented in Fig. 5. The outlined mixer area is 0.13 mm^2 (340 μm by 390 μm). The complete mixer test structure occupies a rectangular surface area of 0.40 mm^2 (650 μm by 610 μm) including LO and RF input balun transformers and the contact pads, which form a significant portion of its area consumption. The four transformers used in the design are identical and they have an inner diameter of 80 μm. The transformers have a single turn in primary and secondary coils, and center taps in both coils for biasing. The transformers use the topmost copper metal layer with a line width of 3.5 μm. The transformers have been designed sufficiently large to enable mixer operation beginning from roughly 60 GHz. Space around the mixer is filled with a mesh structure with multiple metal layers distributing the supply voltages to the mixer, as well as metal-oxide-metal (MOM) bypass capacitors. The structure forms an AC ground at the V_{DD} node as close as possible to the mixer and provides a low-resistance path for supply voltages from the IC contact pads to the circuit to avoid voltage drop in the routing.

IV. Experimental Results

The designed mixer has been manufactured on a shared integrated circuit with stand-alone receiver chain elements. The chip has been designed to allow detailed analysis of each individual element. A measurement PCB has been manufactured and the chip has been wire bonded onto the circuit board for measurements in-house. High-frequency LO and RF signals are fed onto the chip from the sources via 110-GHz cables and on-wafer probes for minimal losses whereas digital SPI signals, supply voltages and biasing reference current are fed onto the chip via PCB traces, connectors, and bond wires, as shown in Fig. 6. The relatively low-frequency IF output signals are also fed out via bond wires, PCB microstrip lines, and connectors, which are appropriately low in losses in the frequency range.

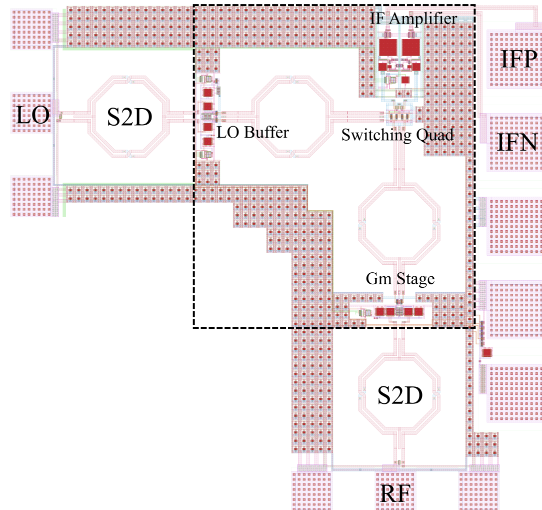

Fig. 5: Mixer layout. The dashed core area is 0.13 mm^2. Extra transformers labeled "S2D" perform the single-ended to differential conversion required for probe measurements.

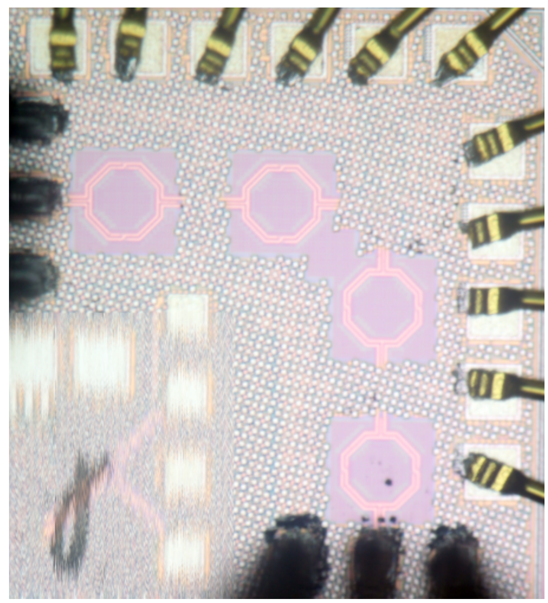

Fig. 6: Microphotograph of the measurement setup. RF and LO signals are fed with probe heads while low-frequency signals and DC power use bond wires.

Fig. 7 presents a block diagram of the high-frequency measurement arrangement. The RF and LO signals are gener-

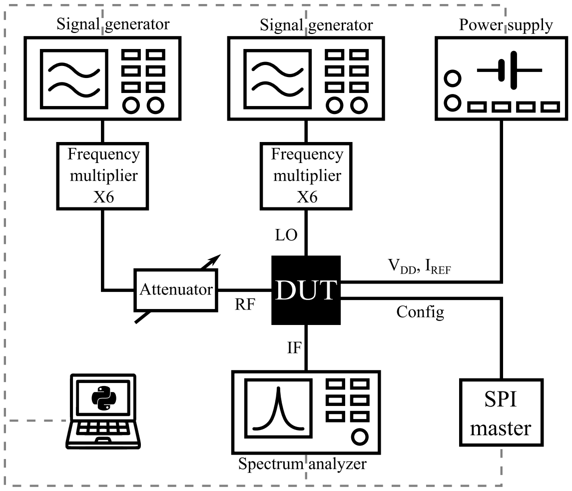

Fig. 7: Mixer measurement setup.

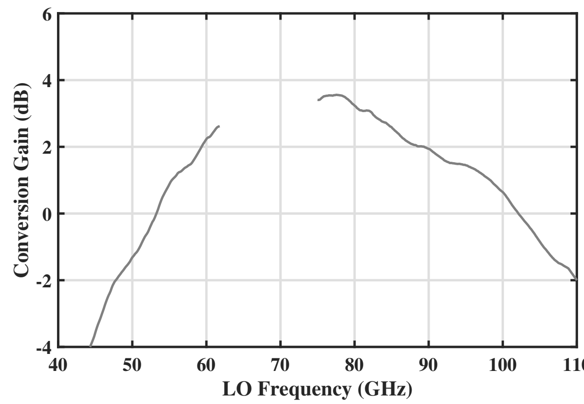

Fig. 8: Measured mixer voltage conversion gain with constant f_{IF} = 1 GHz, and $f_{RF} = f_{LO} + f_{IF}$. The achieved 3-dB RF band is 55 to 100 GHz. The gap in the results is due to a lack of suitable measurement equipment for the frequency range.

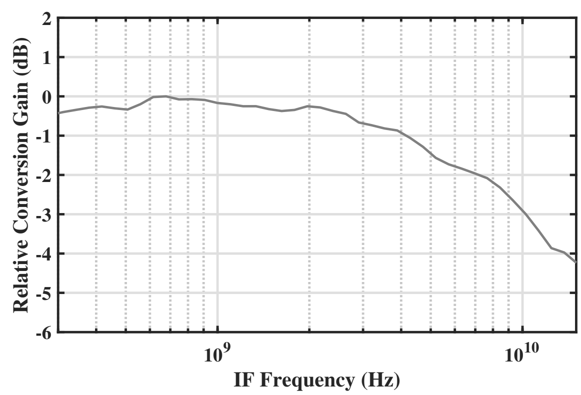

Fig. 9: Measured IF frequency response. Mixer conversion gain is plotted relative to maximum gain. Measured with constant f_{RF} = 80 GHz, and $f_{LO} = f_{RF} + f_{IF}$. The 3-dB IF bandwidth is 10 GHz.

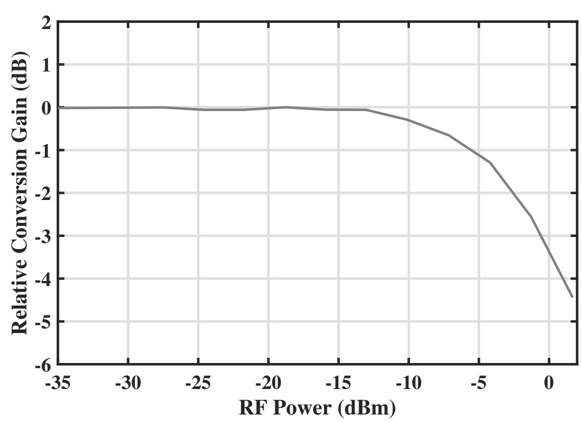

Fig. 10: Mixer compression point measurement. Measured at the mixer conversion gain peak with f_{LO} = 75 GHz, and f_{IF} = 1 GHz. The 1-dB compression point is -6 dBm.

ated with signal generators combined with external frequency multipliers to achieve the desired frequency range for the RF and LO input signals. The two used frequency multipliers are WR10 frequency extension modules, which provide frequency multiplication by a factor of six. The LO signal multiplier has an internal adjustable attenuator and the RF signal multiplier is combined with an external adjustable attenuator to achieve desired signal levels. A DC power supply is used for providing supply voltages and a reference current for biasing, and an external SPI master device has been used for transferring configuring bits onto the chip. The measurement equipment is remotely controlled using Python following The System Development Kit (TheSyDeKick) IC development and testing framework [14].

Measured mixer conversion gain is presented in Fig. 8. The frequency multipliers enable measurements in the frequency range of 75-110 GHz and complementary measurements have been conducted up to 62 GHz using the input signal generators without frequency multipliers. Thus, the measurements have a gap in the frequency range of 62-75 GHz due to the lack of suitable measuring equipment. The measured peak conversion gain is 3.5 dB and the 3-dB RF frequency band is from 54.6 to 100.4 GHz. The measured IF band of the mixer is from 120 MHz to 10.1 GHz. The measured IF frequency response is presented in Fig. 9. The measured DC power consumption is 33.3 mW, out of which the mixer consumes a simulated 16.7 mW of power, the LO buffer consumes 12.0 mW, and the IF amplifier consumes 4.6 mW from a 0.8-V supply. The measured 1-dB compression point is -6 dBm at the mixer input band center frequency of 75 GHz as presented in Fig. 10. Lastly, Table I presents a comparison table of published mmWave mixers. The table clearly demonstrates the existing bandwidth-gain tradeoff and highlights the exceptional wide-band operation and low supply voltage of the mixer designed in this work. The table also verifies that other performance metrics of the proposed mixer are comparable with recently published designs.

Reference	CG (dB)	BW (GHz)	P_{1dB} (dBm)	V_{DD} (V)	P_{DC} (mW)	NF_{DSB} (dB)	Area (mm^2)	Technology	Mixer Topology
This work	**3.5**	**55-100**	**-6**	**0.8**	**33.3**	**13** [1]	**0.13 / 0.40** [2]	**22 nm FDSOI**	**Double-balanced, transformer coupling**
[2] EuMIC 2019	6.5	56-66	-18	2	18	10.5	0.05	22 nm FDSOI	Classic single-balanced, inductorless
[6] RFIC 2020	6	134-149	-	1.4	14	8.8	-	45 nm RFSOI	Double-balanced, series peaking inductors
[9] ISSCC 2020	5.6	55-73	-	0.9	15.2	-	-	28 nm CMOS	Double-balanced, transformer coupling, modified Gm stage
[12] MWCL 2017	5.6	57-66	-7	1	18	7.9	0.22	65 nm CMOS	Double-balanced, transformer coupling, inductive load
[15] TCAS 2021	7	57-67	-9.4	1.2	16	14.4	0.35 [2]	90 nm CMOS	Single-balanced, modified Gm stage, current injection, subharmonic
[16] TCAS 2019	14.6	88-100	-9	1.2	-	11.2	0.36 [2]	90 nm CMOS	Double-balanced, current injection, shunt peaking inductor, active IF load
[17] RWS 2019	17.1	72-100	-13	1.2	4	13.4	0.61 [2]	90 nm CMOS	Double-balanced, series and shunt peaking inductors, modified Gm stage

TABLE I: Comparison table of active mmWave mixers. [1] Simulated NF. [2] Area including pads and input baluns.

V. Acknowledgement

The authors gratefully acknowledge the contributions of Antti Kuhlberg on the PCB manufacturing and chip wire bonding.

VI. Conclusion

This work has presented an active CMOS mmWave mixer design motivated by the high data-rate communication and sensing systems development in the mmWave band. The mixer comprises a modified Gilbert cell active mixer structure, a transformer-loaded common-source LO buffer and a two-stage IF amplifier. The mixer utilizes transformer coupling between its transconductance stage and switching stage to compensate parasitic capacitances, increase voltage headroom and enable individual biasing for the stages. The work has proposed transformer coupling as an especially effective way of improving Gilbert cell mixer performance at mmWave frequencies with the tradeoff of increased area consumption.

The mixer has been implemented in a 22-nm FDSOI CMOS process and its layout area is 0.13 mm^2. The mixer structure achieves a measured peak conversion gain of 3.5 dB and an exceptionally wide 3-dB RF frequency band of 55 GHz to 100 GHz that covers a large range of mmWave communication and sensing bands with a single device. The mixer also demonstrates a wide IF output frequency band of 0.1 - 10 GHz, making the mixer particularly suitable for multi-GHz channel bandwidth mmWave communications applications. It achieves a simulated minimum double sideband noise figure of 13 dB at 1 GHz f_{IF}, and an input 1-dB gain compression point of -6 dBm. The complete mixer structure consumes 33 mW of power from a low 0.8-V supply. The measured performance metrics are competitive with recent published research, and the work verifies the potential of active CMOS Gilbert-cell-based mixer structures even at mmWave frequencies and low supply voltages.

References

[1] A. M. Niknejad and H. Hashemi, *mm-Wave Silicon Technology: 60 GHz and Beyond*, 1st ed. New York, NY: Springer, 2008.

[2] P. Testa, V. Rieß, C. Carta, and F. Ellinger, "An Inductorless 60GHz Down-Conversion Mixer in 22nm FD-SOI CMOS Technology," in *2019 14th European Microwave Integrated Circuits Conference (EuMIC)*, 2019, pp. 152–155.

[3] A. Molnar and C. Andrews, "Impedance, filtering and noise in n-phase passive CMOS mixers," in *Proceedings of the IEEE 2012 Custom Integrated Circuits Conference*, 2012, pp. 1–8.

[4] B. Razavi, "A Millimeter-Wave CMOS Heterodyne Receiver With On-Chip LO and Divider," *IEEE Journal of Solid-State Circuits*, vol. 43, no. 2, pp. 477–485, 2008.

[5] R. Bao, S. Rao, C. Shi, J. Chen, G. Chen, and R. Zhang, "A Ka-Band High-Gain and Wideband mmW Down-Conversion Mixer for 5G Communication Applications," in *2020 IEEE 15th International Conference on Solid-State & Integrated Circuit Technology (ICSICT)*, 2020, pp. 1–3.

[6] S. Li and G. M. Rebeiz, "A 134-149 GHz IF Beamforming Phased-Array Receiver Channel with 6.4-7.5 dB NF Using CMOS 45nm RFSOI," in *2020 IEEE Radio Frequency Integrated Circuits Symposium (RFIC)*, 2020, pp. 103–106.

[7] H.-K. Chiou, K.-C. Lin, W.-H. Chen, and Y.-Z. Juang, "A 1-V 5-GHz Self-Bias Folded-Switch Mixer in 90-nm CMOS for WLAN Receiver," *IEEE Transactions on Circuits and Systems I: Regular Papers*, vol. 59, no. 6, pp. 1215–1227, 2012.

[8] S. Voinigescu, M. Khanpour, S. Nicolson, A. Tomkins, E. Laskin, A. Cathelin, and D. Belot, "CMOS receivers in the 100–140 GHz range," in *2009 IEEE MTT-S International Microwave Symposium Digest*, 2009, pp. 193–196.

[9] A. Chakrabarti, C. Thakkar, S. Yamada, D. Choudhury, J. Jaussi, and B. Casper, "A 64Gb/s 1.4pJ/b/element 60GHz 2×2-Element Phased-Array Receiver with 8b/symbol Polarization MIMO and Spatial Interference Tolerance," in *2020 IEEE International Solid- State Circuits Conference - (ISSCC)*, 2020, pp. 84–86.

[10] S. Shekhar, J. Walling, and D. Allstot, "Bandwidth Extension Techniques for CMOS Amplifiers," *IEEE Journal of Solid-State Circuits*, vol. 41, no. 11, pp. 2424–2439, 2006.

[11] L. Gao and G. M. Rebeiz, "A 20–42-GHz IQ Receiver in 22-nm CMOS FD-SOI With 2.7–4.2-dB NF and -25-dBm IP1dB for Wideband 5G Systems," *IEEE Transactions on Microwave Theory and Techniques*, vol. 69, no. 11, pp. 4951–4960, 2021.

[12] C. Choi, J. H. Son, O. Lee, and I. Nam, "A +12-dBm OIP3 60-GHz RF Downconversion Mixer With an Output-Matching, Noise- and Distortion-Canceling Active Balun for 5G Applications," *IEEE*

Microwave and Wireless Components Letters, vol. 27, no. 3, pp. 284–286, 2017.

[13] R. Carter, J. Mazurier, L. Pirro, J.-U. Sachse, P. Baars, J. Faul, C. Grass, G. Grasshoff, P. Javorka, T. Kammler, A. Preusse, S. Nielsen, T. Heller, J. Schmidt, H. Niebojewski, P.-Y. Chou, E. Smith, E. Erben, C. Metze, C. Bao, Y. Andee, I. Aydin, S. Morvan, J. Bernard, E. Bourjot, T. Feudel, D. Harame, R. Nelluri, H.-J. Thees, L. M-Meskamp, J. Kluth, R. Mulfinger, M. Rashed, R. Taylor, C. Weintraub, J. Hoentschel, M. Vinet, J. Schaeffer, and B. Rice, "22nm FDSOI technology for emerging mobile, Internet-of-Things, and RF applications," in *2016 IEEE International Electron Devices Meeting (IEDM)*, 2016, pp. 2.2.1–2.2.4.

[14] M. Kosunen, "TheSyDeKick - Complete Kit for System-on-Chip development," accessed 28 August 2023. [Online]. Available: https://github.com/TheSystemDevelopmentKit

[15] Y.-T. Chang, C.-Y. Kang, and H.-C. Lu, "A V-Band High Gain Sub-Harmonic Down-Conversion Mixer Using PMOS Cross Couple Pair to Implement Negative Impedance and Current-Bleeding Technique," *IEEE Transactions on Circuits and Systems II: Express Briefs*, vol. 68, no. 8, pp. 2765–2769, 2021.

[16] Y.-S. Lin and Y. E. Wang, "Design and Analysis of a 94-GHz CMOS Down-Conversion Mixer With CCPT-RL-Based IF Load," *IEEE Transactions on Circuits and Systems I: Regular Papers*, vol. 66, no. 8, pp. 3148–3161, 2019.

[17] Y.-S. Lin, K.-S. Lan, and J.-Y. Liao, "W-Band CMOS Down-Conversion Mixer Using CMOS-Inverter -Based RF GM Stage for Gain and Linearity Enhancement," in *2019 IEEE Radio and Wireless Symposium (RWS)*, 2019, pp. 1–4.